

Recent Results on Spectroscopy from COMPASS

Boris Grube^{1,a)} for the COMPASS Collaboration

¹*Physik-Department E18, Technische Universität München, Garching, Germany*

^{a)}Corresponding author: bgrube@tum.de

Abstract. The COMmon Muon and Proton Apparatus for Structure and Spectroscopy (COMPASS) is a multi-purpose fixed-target experiment at the CERN Super Proton Synchrotron (SPS) aimed at studying the structure and spectrum of hadrons. The two-stage spectrometer has a good acceptance for charged as well as neutral particles over a wide kinematic range and is thus able to measure a wide range of reactions. Light mesons are studied with negative (mostly π^-) and positive (p , π^+) hadron beams with a momentum of 190 GeV/c. The light-meson spectrum is investigated in various final states produced in diffractive dissociation reactions at squared four-momentum transfers to the target between 0.1 and 1.0 (GeV/c)². The flagship channel is the $\pi^-\pi^+\pi^-$ final state, for which COMPASS has recorded the currently largest data sample. These data not only allow for measuring the properties of known resonances with high precision, but also for searching for new states. Among these is a new resonance-like signal, the $a_1(1420)$, with unusual properties. The findings are confirmed by the analysis of the $\pi^-\pi^0\pi^0$ final state. Possible bias introduced by the parametrizations used to describe the $\pi\pi$ S -wave is studied using a novel analysis technique, which extracts the amplitude of the $\pi^+\pi^-$ sub-system as a function of 3π mass from the data. Of particular interest is the resonance content of the partial wave with spin-exotic $J^{PC} = 1^{-+}$ quantum numbers, which are forbidden for quark-antiquark states. This wave is studied in the two 3π channels. Further insight is gained by studying diffractively produced $\pi^-\eta$ or $\pi^-\eta'$ final states.

INTRODUCTION

The COMPASS experiment [1] has recorded large data sets of diffractive dissociation reactions of the type $\pi^- + p \rightarrow X^- + p_{\text{recoil}}$ using a 190 GeV/c pion beam on a liquid-hydrogen target. In this process, the beam hadron is excited to some intermediate state X^- via t -channel Reggeon exchange with the target. At 190 GeV/c beam momentum pomeron exchange is dominant. Diffractive reactions are known to exhibit a rich spectrum of intermediate states X^- . In the past, several candidates for spin-exotic mesons have been reported in pion-induced diffraction [2, 3]. The mesonic states X^- decay into various multi-hadron final states, which are detected by the spectrometer. Here, we consider the $\pi^-\eta$, $\pi^-\eta'$, $\pi^-\pi^+\pi^-$, and $\pi^-\pi^0\pi^0$ channels. In order to disentangle the different contributing intermediate states X^- , for each final state a partial-wave analysis (PWA) is performed. In addition to the final-state particles from the X^- decays, the recoiling proton is also measured. This helps to suppress backgrounds and ensures an exclusive measurement by applying energy and momentum conservation in the event selection.

The scattering process is characterized by two kinematic variables: the squared total center-of-mass energy s and the squared four-momentum transfer to the target $t = (p_{\text{beam}} - p_X)^2 < 0$. It is customary to use the reduced four-momentum transfer $t' \equiv |t| - |t|_{\text{min}}$ instead of t , where $|t|_{\text{min}}$ is the minimum value of $|t|$ for a given invariant mass of X^- . The analyses presented are all performed in the range $0.1 < t' < 1.0$ (GeV/c)².

PARTIAL-WAVE ANALYSIS OF THE $\pi^-\eta$ AND $\pi^-\eta'$ FINAL STATES

The $\pi^-\eta$ and $\pi^-\eta'$ final states are interesting, because in both channels the odd-spin partial waves have spin-exotic J^{PC} quantum numbers that are forbidden for quark-antiquark states in the non-relativistic limit. By convention, the C -parity is that of the neutral partner of the X^- in the isospin triplet. A comparison of the two channels also gives insight into the role of flavor symmetry. The η is reconstructed via its decay into $\pi^+\pi^-\pi^0$, where $\pi^0 \rightarrow \gamma\gamma$. For the η' , its decay into $\pi^+\pi^-\eta$ with $\eta \rightarrow \gamma\gamma$ is used.

The partial-wave analysis of the two channels [4] is performed in 40 MeV/c² wide bins of the final-state invariant mass and makes therefore no assumptions on the resonance content of the partial waves. The two-body decay of the

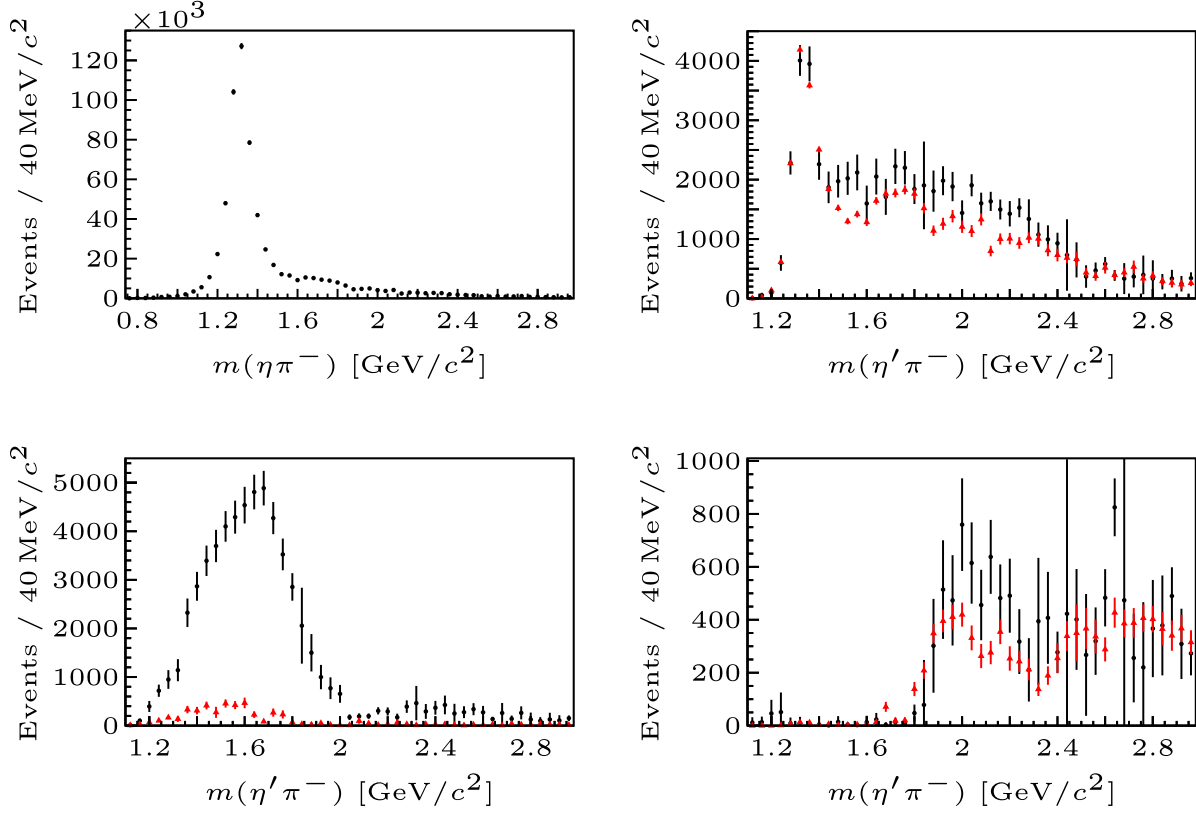


FIGURE 1. Top left: intensity of the D wave with $J^{PC} = 2^{++}$ in the $\pi^- \eta$ final state. The other three panels show in black the intensities of the 2^{++} (D wave; top right), 1^{+} (P wave; bottom left), and 4^{++} (G wave; bottom right) $\pi^- \eta'$ waves. The red data points represent the corresponding $\pi^- \eta$ intensities scaled by Eq. (1). Figures from Ref. [4].

X^- is described in the Gottfried-Jackson frame by spherical harmonics. The partial waves are defined by the orbital angular momentum L between the pion and the $\eta^{(\prime)}$, which corresponds to the spin J of the X^- , by the absolute value M of the spin projection, and by the reflectivity $\epsilon = \pm 1$, which corresponds to the naturality of the exchanged particle. Partial waves with $\epsilon = -1$ are found to be negligibly small, except for the S wave with $M = 0$, which contributes 0.5% in the $\pi^- \eta$ and 1.1% in the $\pi^- \eta'$ channel. This is in agreement with the expected pomeron dominance at high energies. For positive reflectivity (naturality), only waves with $M \geq 1$ are allowed so that $L = J \geq 1$. The data are dominated by $M = 1$ partial waves. The PWA model includes $M = 1$ waves with $L = 1$ to 6. Higher M states are suppressed. Only the $\pi^- \eta$ D wave shows significant intensity for $M = 2$.

The $\pi^- \eta$ data are dominated by the D wave with a prominent peak corresponding to the $a_2(1320)$ (see Fig. 1 top left). In contrast, the D wave is much weaker in the $\pi^- \eta'$ channel (black data points in Fig. 1 top right). However, in the quark-line picture and assuming point-like resonances, the $\pi^- \eta$ and $\pi^- \eta'$ intensities for a partial wave with spin J should be related by the ratios of phase space and angular-momentum barrier factors and by the branching-fraction ratio B for η and η' decaying to $\pi^+ \pi^- \gamma \gamma$:

$$N_J^{\pi \eta'}(m) \propto B \left[\frac{q^{\pi \eta'}(m)}{q^{\pi \eta}(m)} \right]^{2J+1} N_J^{\pi \eta}(m) \quad (1)$$

Here N_J is the acceptance-corrected number of events in the partial wave with spin J of the respective final state and q is the corresponding breakup momentum.

Scaling the $\pi^- \eta$ partial-wave intensities according to Eq. (1) (red data points in Fig. 1) yields for even-spin waves intensity distributions that are quite similar to those in the $\pi^- \eta'$ channel (see Fig. 1 right column). This is consistent with the assumption that in both channels the intermediate states X^- couple to the same final-state flavor content. It is

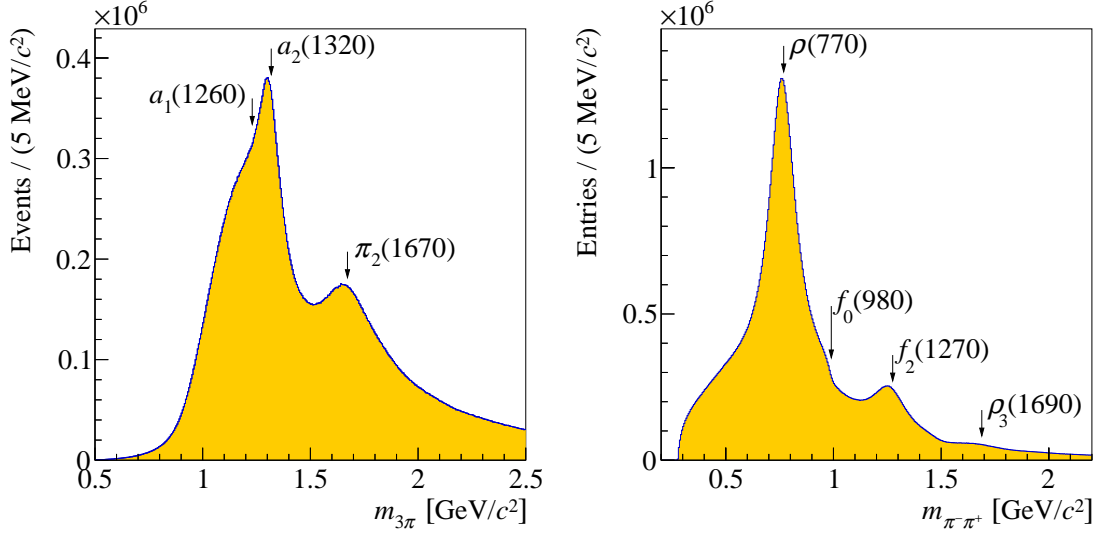


FIGURE 2. Left: $\pi^-\pi^+\pi^-$ invariant mass spectrum in the analyzed range; Right: invariant mass distribution of the $\pi^+\pi^-$ subsystem (two entries per event). Figures from Ref. [9].

interesting to note that the similarities in the even-spin waves are not limited to the resonance regions, i.e. $a_2(1320)$ in the D and $a_4(2040)$ in the G wave. Similar intensity distributions are also observed in the high-mass regions, which contain large non-resonant contributions. The picture is completely different for the spin-exotic odd-spin partial waves. The scaled $\pi^-\eta$ partial-wave intensities are suppressed by factors of 5 to 10 compared to $\pi^-\eta'$. This is illustrated in Fig. 1 bottom left for the $J^{PC} = 1^{-+}$ wave, which is the dominant wave in the $\pi^-\eta'$ channel.

Resonance-model fits using relativistic Breit-Wigner amplitudes yield resonance parameters for the $a_2(1320)$ and the $a_4(2040)$ that are consistent with PDG values [5]. From these fits the following branching-fraction ratios are extracted:

$$B_2 \equiv \frac{N(a_2 \rightarrow \pi^-\eta')}{N(a_2 \rightarrow \pi^-\eta)} = (5 \pm 2)\% \quad \text{and} \quad B_4 \equiv \frac{N(a_4 \rightarrow \pi^-\eta')}{N(a_4 \rightarrow \pi^-\eta)} = (23 \pm 7)\%$$

Here the N are the integrated Breit-Wigner intensities for the respective decays. The ratio B_2 is in agreement with previous measurements; B_4 is measured for the first time. For the spin-exotic P waves, the results of the resonance-model fit are strongly model dependent. Applying the models of previous analyses [6, 7, 8] yields similar resonance parameters for the $\pi_1(1400)$ in $\pi^-\eta$ and for the $\pi_1(1600)$ in $\pi^-\eta'$. However, the results depend on the modeling of the D waves above the $a_2(1320)$ and on the parametrization of the non-resonant component in the P waves. Both have to be better understood before firm conclusions can be drawn about the resonance content of the P waves.

PARTIAL-WAVE ANALYSIS OF THE $\pi^-\pi^+\pi^-$ AND $\pi^-\pi^0\pi^0$ FINAL STATES

After all the selection cuts, the 3π data samples consist of 46×10^6 $\pi^-\pi^+\pi^-$ and 3.5×10^6 $\pi^-\pi^0\pi^0$ exclusive events in the analyzed kinematic region of three-pion mass, $0.5 < m_{3\pi} < 2.5$ GeV/c^2 . Figure 2 shows the $\pi^-\pi^+\pi^-$ mass spectrum together with that of the $\pi^+\pi^-$ subsystem. The known pattern of resonances $a_1(1260)$, $a_2(1320)$, and $\pi_2(1670)$ is seen in the 3π system along with $\rho(770)$, $f_0(980)$, $f_2(1270)$, and $\rho_3(1690)$ in the $\pi^+\pi^-$ subsystem.

Partial-Wave Decomposition

The PWA of the $(3\pi)^-$ final states is based on the isobar model, which assumes that the X^- decays first into an intermediate resonance, which is called the isobar, and a ‘‘bachelor’’ pion (π^- for the $\pi^-\pi^+\pi^-$ final state; π^0 for $\pi^-\pi^0\pi^0$). In a second step, the isobar decays into two pions. In accordance with the $\pi^+\pi^-$ invariant mass spectrum shown in Fig. 2 right and with analyses by previous experiments, we include $[\pi\pi]_S$, $\rho(770)$, $f_0(980)$, $f_2(1270)$, $f_0(1500)$, and $\rho_3(1690)$ as isobars into the fit model. Here, $[\pi\pi]_S$ represents the broad component of the $\pi\pi$ S -wave. Based on the

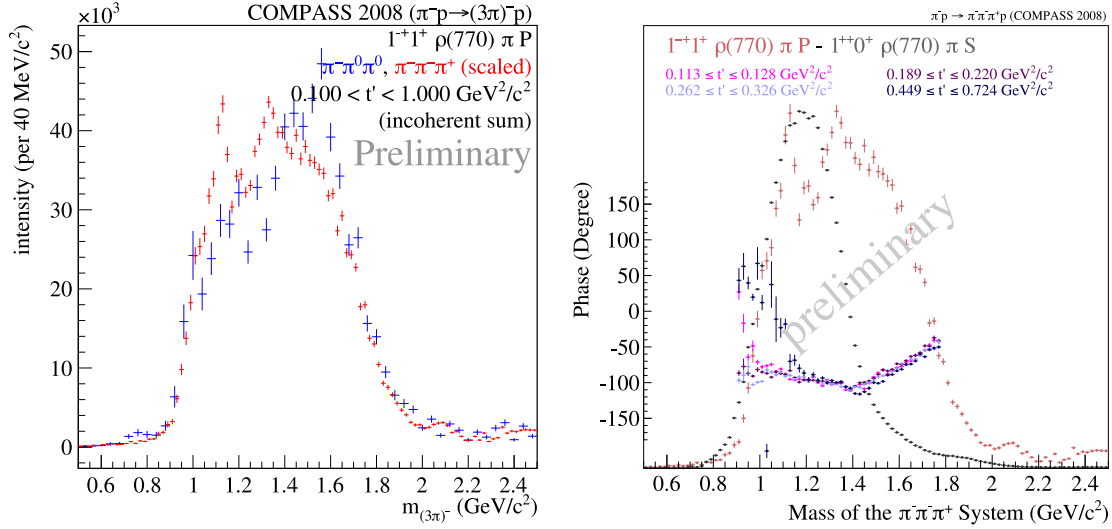


FIGURE 3. Left: Intensity of the $1^{-+} 1^{+} \rho(770) \pi P$ wave summed over all t' bins for the $\pi^{-} \pi^{+} \pi^{-}$ (red) and the $\pi^{-} \pi^{0} \pi^{0}$ (blue) final state. Right: Phase of the $1^{-+} 1^{+} \rho(770) \pi P$ wave relative to the $1^{++} 0^{+} \rho(770) \pi S$ wave for four t' bins in the $\pi^{-} \pi^{+} \pi^{-}$ data. The black and dark red points show the shapes of the intensity distributions of the two waves scaled to the same height.

six isobars, we have constructed a set of partial waves that consists of 88 waves in total, including one non-interfering isotropic wave representing three uncorrelated pions. This constitutes the largest wave set ever used in an analysis of the 3π final state. The partial-wave decomposition is performed in narrow bins of the 3π invariant mass. Since the data show a complicated correlation of the $m_{3\pi}$ and t' spectra, each $m_{3\pi}$ bin is further subdivided into non-equidistant bins in the four-momentum transfer t' . For the $\pi^{-} \pi^{+} \pi^{-}$ channel 11 bins are used, for the $\pi^{-} \pi^{0} \pi^{0}$ final state 8 bins. With this additional binning in t' , the dependence of the partial-wave amplitudes on the four-momentum transfer can be studied in detail. The details of the analysis model are described in Ref. [9].

The partial-wave amplitudes are extracted from the data as a function of $m_{3\pi}$ and t' by fitting the five-dimensional kinematic distributions of the outgoing three pions. The amplitudes do contain information not only about the partial-wave intensities, but also about the relative phases of the partial waves. The latter are crucial for resonance extraction. Three-pion partial waves are defined by the quantum numbers of the X^{-} (spin J , parity P , C -parity, absolute value M of the spin projection), the naturality $\epsilon = \pm 1$ of the exchange particle, the isobar, and the orbital angular momentum L between the isobar and the bachelor pion. These quantities are summarized in the partial-wave notation $J^{PC} M^{\epsilon}$ [isobar] πL . Since at the used beam energies pomeron exchange is dominant, 80 of the 88 partial waves in the model have $\epsilon = +1$.

The $J^{PC} = 1^{-+}$ Spin-Exotic Wave

The 88-wave model also contains waves with spin-exotic J^{PC} quantum numbers. The most interesting of these waves is the $1^{-+} 1^{+} \rho(770) \pi P$ wave, which contributes less than 1% to the total intensity. Previous analyses claimed a resonance, the $\pi_1(1600)$, at about $1.6 \text{ GeV}/c^2$ in this channel [10, 11]. Figure 3 left shows the intensity of this partial wave for the two final states ($\pi^{-} \pi^{+} \pi^{-}$ in red, $\pi^{-} \pi^{0} \pi^{0}$ in blue). The two distributions are scaled to have the same integral. Both decay channels are in fair agreement and exhibit a broad enhancement extending from about 1.0 to $1.8 \text{ GeV}/c^2$ in $m_{3\pi}$. In the 1.0 to $1.2 \text{ GeV}/c^2$ mass range the intensity depends strongly on the details of the fit model. Peak-like structures in this region are probably due to imperfections of the applied PWA model.

A remarkable change of the shape of the intensity spectrum of the $1^{-+} 1^{+} \rho(770) \pi P$ wave with t' is observed (see Fig. 4). At values of t' below about $0.3 \text{ (GeV}/c^2)^2$, we observe no indication of a resonance peak around $m_{3\pi} = 1.6 \text{ GeV}/c^2$, where we would expect the $\pi_1(1600)$. For the t' bins in the interval from 0.449 to $1.000 \text{ (GeV}/c^2)^2$, the observed intensities exhibit a very different shape as compared to the low- t' region, with a peak structure emerging at about $1.6 \text{ GeV}/c^2$ and the intensity at lower masses disappearing rapidly with increasing t' . This is in contrast to clean resonance signals like the $a_2(1320)$ in the $2^{++} 1^{+} \rho(770) \pi D$ wave, which, as expected, do not change their shape with

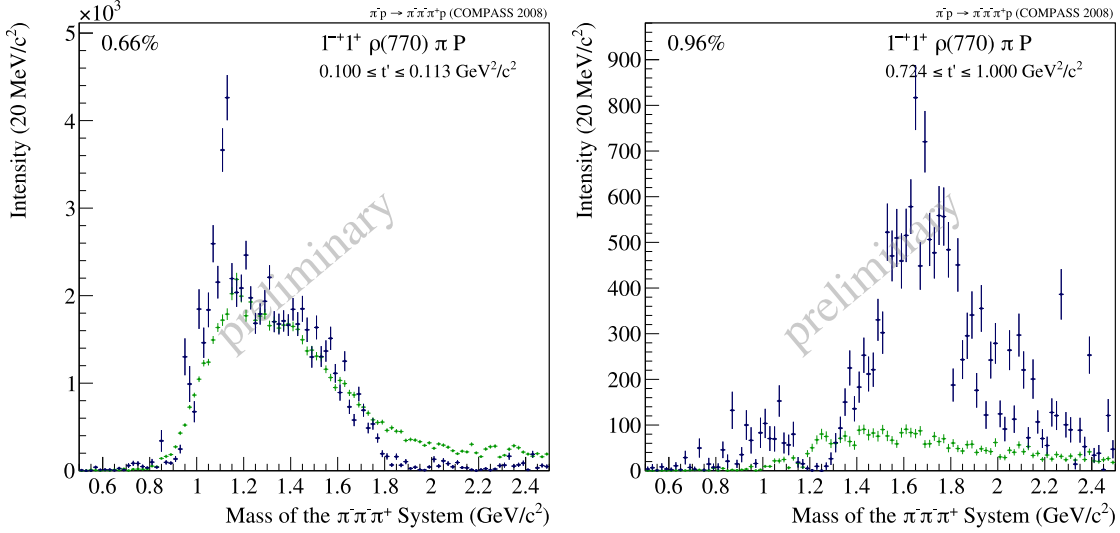


FIGURE 4. Intensity of the $1^{-+} 1^{+} \rho(770) \pi P$ wave in different regions of t' (left: low t' ; right: high t') for the $\pi^{-} \pi^{+} \pi^{-}$ final state (dark blue). The partial-wave projections of Monte-Carlo data generated according to a model of the Deck effect are overlaid in green.

t' . The observed t' behavior of the 1^{-+} intensity is therefore a strong indication that non-resonant contributions play a dominant role. Interestingly, the relative phases of the $1^{-+} 1^{+} \rho(770) \pi P$ wave with respect to other waves are virtually independent of t' . As an example, Fig. 3 right shows the phase relative to the $1^{++} 0^{+} \rho(770) \pi S$ wave for four t' bins. In all bins, a slowly rising phase with a total phase motion of about 60° is observed around the $1.6 \text{ GeV}/c^2$ region.

It is believed that the non-resonant contribution in the 1^{-+} wave originates predominantly from the Deck effect, in which the incoming beam pion dissociates into the isobar and an off-shell pion that scatters off the target proton to become on-shell [12]. As a first step towards a better understanding of the non-resonant contribution, Monte-Carlo data were generated that are distributed according to a model of the Deck effect. The model employed here is very similar to that used in Ref. [13]. The partial-wave projection of these Monte Carlo data is shown as green points in Fig. 4. In order to compare the intensities of real data and the Deck-model pseudo data, the Monte Carlo data are scaled to the t' -summed intensity of the 1^{-+} wave as observed in real data. At values of t' below about $0.3 (\text{GeV}/c)^2$, the intensity distributions of real data and Deck Monte Carlo exhibit strong similarities suggesting that the observed intensity might be saturated by the Deck effect. Starting from $t' \approx 0.4 (\text{GeV}/c)^2$, the spectral shapes for Deck pseudo-data and real data deviate from each other with the differences increasing towards larger values of t' . This leaves room for a potential resonance signal. It should be noted, however, that the Deck pseudo data contain no resonant contributions. Therefore, potential interference effects between the resonant and non-resonant amplitudes cannot be assessed in this simple approach.

The $a_1(1420)$

A surprising find in the COMPASS data was a pronounced narrow peak at about $1.4 \text{ GeV}/c^2$ in the $1^{++} 0^{+} f_0(980) \pi P$ wave (see Fig. 5). The peak is observed with similar shape in the $\pi^{-} \pi^{+} \pi^{-}$ and $\pi^{-} \pi^0 \pi^0$ data and is robust against variations of the PWA model. In addition to the peak in the partial-wave intensity, rapid phase variations with respect to most waves are observed in the $1.4 \text{ GeV}/c^2$ region (see Fig. 6). The phase motion as well as the peak shape change only little with t' .

In order to test the compatibility of the signal with a Breit-Wigner resonance, a resonance-model fit was performed using a novel method, where the intensities and relative phases of three waves ($1^{++} 0^{+} f_0(980) \pi P$, $2^{++} 1^{+} \rho(770) \pi D$, and $4^{++} 1^{+} \rho(770) \pi G$) were fit simultaneously in all 11 t' bins [14]. Forcing the resonance parameters to be the same across all t' bins leads to an improved separation of resonant and non-resonant contribution as compared to previous analyses that did not incorporate the t' information. The Breit-Wigner model describes the peak in the $1^{++} 0^{+} f_0(980) \pi P$ wave well and yields a mass of $m_0 = 1414_{-13}^{+15} \text{ MeV}/c^2$ and a width of $\Gamma_0 = (153_{-23}^{+8}) \text{ MeV}/c^2$

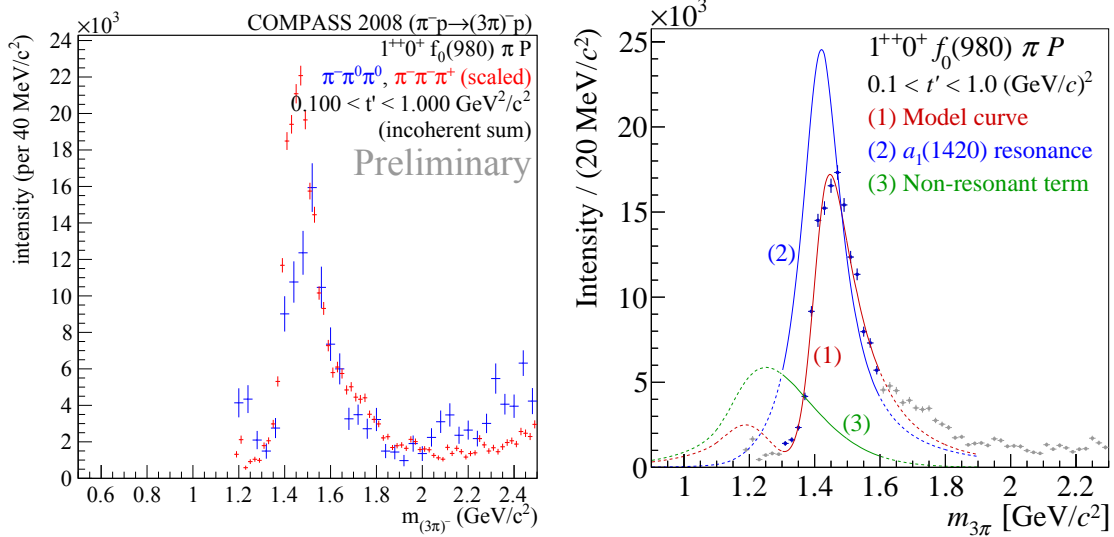


FIGURE 5. Left: Intensity of the $1^{++}0^+ f_0(980)\pi P$ wave summed over all t' bins for the $\pi^-\pi^+\pi^-$ (red) and the $\pi^-\pi^0\pi^0$ (blue) final states. Right: Result of a resonance-model fit to the $\pi^-\pi^+\pi^-$ data [14]. The data points correspond to the red points in the left figure.

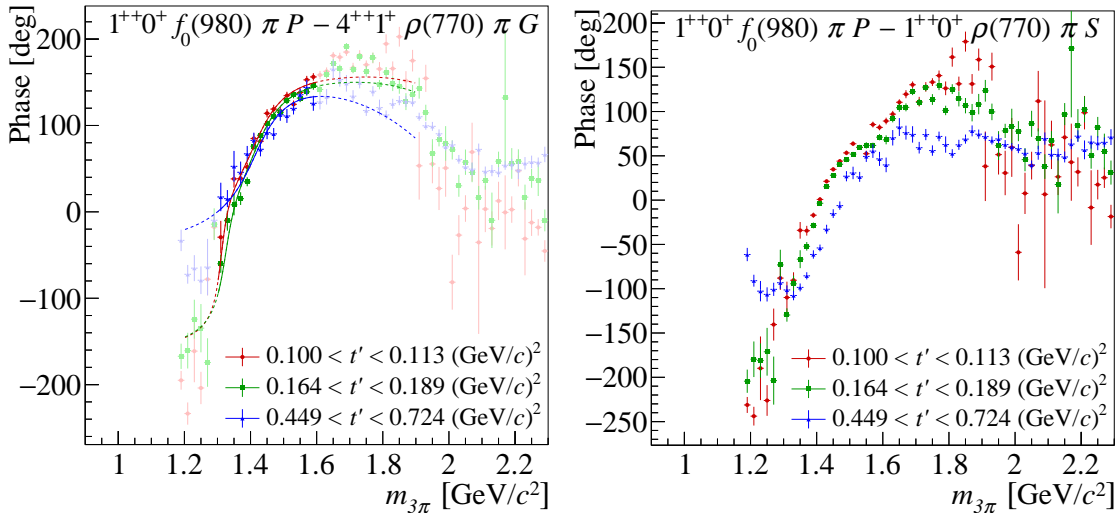


FIGURE 6. Examples for relative phases of the $1^{++}0^+ f_0(980)\pi P$ wave with respect to the $4^{++}1^+ \rho(770)\pi G$ (left) and the $1^{++}0^+ \rho(770)\pi S$ wave (right). The phases are shown for three different t' regions indicated by the color. Figures from Ref. [14].

for the $a_1(1420)$. Due to the high statistical precision of the data, the uncertainties are dominated by systematic effects.

The $a_1(1420)$ signal is remarkable in many ways. It appears in a mass region that is well studied since decades. However, previous experiments were unable to see the peak, because it contributes only 0.25% to the total intensity. The $a_1(1420)$ is very close in mass to the 1^{++} ground state, the $a_1(1260)$. But it has a much smaller width than the $a_1(1260)$. The $a_1(1420)$ peak is seen only in the $f_0(980)\pi$ decay mode of the 1^{++} waves and lies suspiciously close to the $K \bar{K}^*(892)$ threshold.

The nature of the $a_1(1420)$ is still unclear and several interpretations were proposed. It could be the isospin partner to the $f_1(1420)$. It was also described as a two-quark-tetraquark mixed state [15] and a tetraquark with mixed flavor symmetry [16]. Other models do not require an additional resonance: Ref. [17, 18] proposes resonant re-scattering corrections in the Deck process as an explanation, whereas Ref. [19] suggests a branching point in the triangle rescat-

tering diagram for $a_1(1260) \rightarrow K \bar{K}^*(892) \rightarrow K \bar{K} \pi \rightarrow f_0(980)\pi$. More detailed studies are needed in order to distinguish between these models.

Extraction of $\pi\pi$ S-Wave Isobar Amplitudes from Data

The PWA of the 3π system is based on the isobar model, where fixed amplitudes are used for the description of the $\pi^+\pi^-$ intermediate states. However, we cannot exclude that the fit results are biased by the employed isobar parametrizations. This is true in particular for the isoscalar $J^{PC} = 0^{++}$ isobars. In the PWA model, a broad $\pi\pi$ S-wave component is used, the parametrization of which is extracted from $\pi\pi$ S-wave elastic-scattering data [20]. In addition, the $f_0(980)$, described by a Flatté form [21], and the $f_0(1500)$, parametrized by a relativistic Breit-Wigner amplitude, are included as isobars. In order to study possible bias due to these parametrizations and to ensure that the observed $a_1(1420)$ signal is truly related to the narrow $f_0(980)$, a novel analysis method [9] inspired by Ref. [22] was developed. In this so-called *freed-isobar* analysis, the three fixed parametrizations for the 0^{++} isobar amplitudes are replaced by a set of piecewise constant complex-valued functions that fully cover the allowed two-pion mass range. This way the whole 0^{++} isobar amplitude is extracted as a function of the 3π mass. In contrast to the conventional isobar approach, which uses the same isobar parametrization in different partial waves, the freed-isobar method permits different isobar amplitudes for different intermediate states X^- . A more detailed description of the analysis method can be found in Ref. [9].

The freed-isobar method leads to a reduced model dependence and gives additional information about the $\pi^+\pi^-$ subsystem at the cost of a considerable increase in the number of free parameters in the PWA fit. Thus, even for large data sets, the freed-isobar approach can only be applied to a subset of partial waves. We performed a freed-isobar PWA, where the fixed parametrizations of the broad $\pi\pi$ S-wave component, of the $f_0(980)$, and of the $f_0(1500)$ were replaced by piece-wise constant isobar amplitudes for the 3π partial waves $0^{-+} 0^+ [\pi\pi]_{0^{++}} \pi S$, $1^{++} 0^+ [\pi\pi]_{0^{++}} \pi P$, and $2^{-+} 0^+ [\pi\pi]_{0^{++}} \pi D$. Figure 7 top shows the two-dimensional intensity distribution of the $1^{++} 0^+ [\pi\pi]_{0^{++}} \pi P$ wave as a function of $m_{\pi^+\pi^-}$ and $m_{3\pi}$. The distribution exhibits a broad maximum around $m_{3\pi} = 1.2 \text{ GeV}/c^2$ and between 0.6 and 0.8 GeV/c^2 in $m_{\pi^+\pi^-}$. A smaller peak is observed in the $f_0(980)$ region at $m_{3\pi} \approx 1.4 \text{ GeV}/c^2$. This peak is more obvious in Fig. 7 bottom left, which shows the intensity distribution summed over the two-pion mass interval around the $f_0(980)$ as indicated by the pair of horizontal dashed lines in Fig. 7 top. The peak is similar in position and shape to the $a_1(1420)$ peak in the $1^{++} 0^+ f_0(980)\pi P$ wave (cf. Fig. 5). The resonant nature of the $f_0(980)$ becomes apparent in Fig. 7 bottom right, which shows the $m_{\pi^+\pi^-}$ dependence of the extracted amplitude at the $a_1(1420)$ peak in form of an Argand diagram. The phase is measured with respect to the $1^{++} 0^+ \rho(770)\pi S$ wave. The $f_0(980)$ contribution shows up as a semicircle-like structure (highlighted by the blue line) with a shifted origin. This demonstrates that the observed $a_1(1420)$ signal in the $f_0(980)\pi$ decay mode is not an artifact of the 0^{++} isobar parametrizations used in the conventional PWA method. More results of the freed-isobar PWA are discussed in Refs. [9, 23].

ACKNOWLEDGMENTS

This work was supported by the BMBF, the MLL and the Cluster of Excellence Exc153 “Origin and Structure of the Universe”.

REFERENCES

- [1] P. Abbon *et al.* (COMPASS Collaboration), Nucl. Instrum. Methods Phys. Res., Sect. A **779**, p. 69 (2015).
- [2] C. Meyer *et al.*, Phys. Rev. C **82**, p. 025208 (2010).
- [3] E. Klempt *et al.*, Phys. Rept. **454**, p. 1 (2007).
- [4] C. Adolph *et al.* (COMPASS Collaboration), Phys. Lett. B **740**, p. 303 (2015).
- [5] J. Beringer *et al.* (Particle Data Group), Phys. Rev. D **86**, p. 010001 (2012).
- [6] S.-U. Chung *et al.* (E852 Collaboration), Phys. Rev. D **60**, p. 092001 (1999).
- [7] E. I. Ivanov *et al.* (E852 Collaboration), Phys. Rev. Lett. **86**, p. 3977 (2001).
- [8] V. Dorofeev *et al.* (VES Collaboration), AIP Conf. Proc. **619**, p. 143 (2002).
- [9] C. Adolph *et al.* (COMPASS Collaboration), arXiv:1509.00992, *submitted to Phys. Rev. D* (2015).
- [10] S.-U. Chung *et al.* (E852 Collaboration), Phys. Rev. D **60**, p. 092001 (1999).
- [11] M. Alekseev *et al.* (COMPASS Collaboration), Phys. Rev. Lett. **104**, p. 241803 (2010).

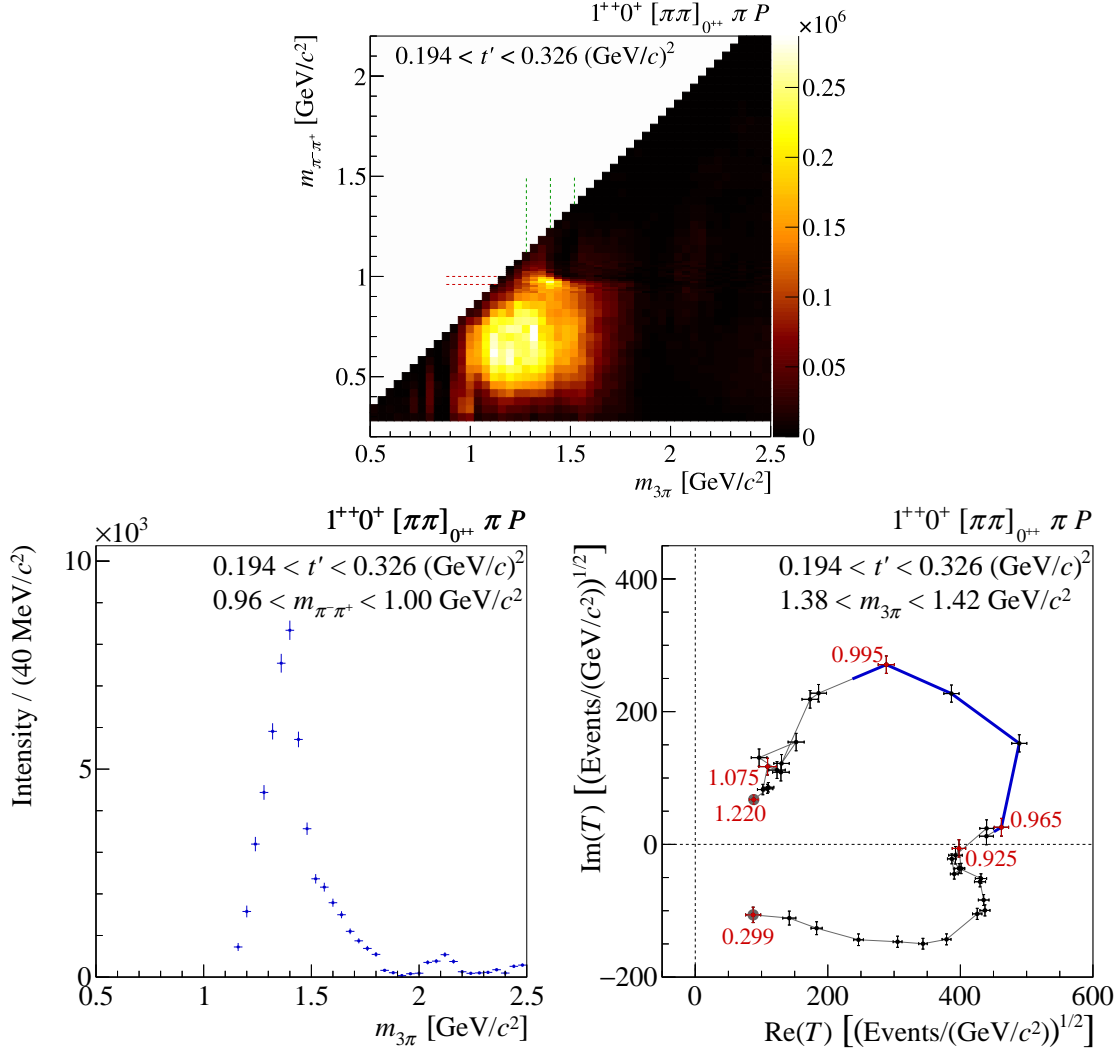


FIGURE 7. Intensity of the $\pi\pi$ S-wave component of the $J^{PC} M^\epsilon = 1^{++} 0^+$ partial wave resulting from the freed-isobar fit. Top: two-dimensional representation of the partial-wave intensity as a function of $m_{\pi^+\pi^-}$ and $m_{3\pi}$. Bottom left: intensity as a function of $m_{3\pi}$ summed over the $m_{\pi^+\pi^-}$ interval around the $f_0(980)$ indicated by the pair of horizontal dashed lines in the top figure. Bottom right: Argand diagram representing the $m_{\pi^+\pi^-}$ dependence of the partial-wave amplitude for the 3π mass bin at the $a_1(1420)$ measured with respect to the $1^{++} 0^+ \rho(770)\pi S$ wave. Figures from Ref. [9].

- [12] R. T. Deck, Phys. Rev. Lett. **13**, p. 169 (1964).
- [13] C. Daum *et al.* (ACCMOR Collaboration), Nucl. Phys. B **182**, p. 269 (1981).
- [14] C. Adolph *et al.* (COMPASS Collaboration), Phys. Rev. Lett. **115**, p. 082001 (2015).
- [15] Z.-G. Wang, arXiv:1401.1134 (2014).
- [16] H.-X. Chen *et al.*, Phys. Rev. D **91**, p. 094022 (2015).
- [17] J.-L. Basdevant and E. L. Berger, Phys. Rev. Lett. **114**, p. 192001 (2015).
- [18] J.-L. Basdevant and E. L. Berger, arXiv:1501.04643 (2015).
- [19] M. Mikhasenko *et al.*, Phys. Rev. D **91**, p. 094015 (2015).
- [20] K. L. Au, D. Morgan, and M. R. Pennington, Phys. Rev. D **35**, p. 1633 (1987).
- [21] M. Ablikim *et al.* (BES Collaboration), Phys. Lett. B **607**, p. 243 (2005).
- [22] E. M. Aitala *et al.* (E791 Collaboration), Phys. Rev. D **73**, p. 032004 (2006).
- [23] F. Krinner, in these Proceedings .